

# Structure-Property Relationships of Hydrogel-based Atmospheric Water Harvesting Systems

An Feng,<sup>[a]</sup> Yihan Shi,<sup>[a]</sup> Casey Onggowarsito,<sup>[a]</sup> Xin Stella Zhang,<sup>[a]</sup> Shudi Mao,<sup>[a]</sup> Muhammed A.H. Johir,<sup>[a]</sup> Qiang Fu,<sup>\*[a]</sup> and Long D. Nghiem<sup>[a]</sup>

Atmospheric water harvesting (AWH) is considered one of the promising technologies to alleviate the uneven-distribution of water resources and water scarcity in arid regions of the world. Hydrogel-based AWH materials are currently attracting increasing attention due to their low cost, high energy efficiency and simple preparation. However, there is a knowledge gap in the screening of hydrogel-based AWH materials in terms of structure-property relationships, which may increase the cost of trial and error in research and fabrication. In this study, we synthesised a variety of hydrogel-based AWH materials, charac-

terized their physicochemical properties visualized the electrostatic potential of polymer chains, and ultimately established the structure-property-application relationships of polymeric AWH materials. Poly(2-acrylamido-2-methyl-1-propanesulfonic acid) (PAMPS) hydrogel is able to achieve an excellent water adsorption capacity of  $0.62 \text{ g g}^{-1}$  and a high water desorption efficiency of more than 90% in relatively low-moderate humidity environments, which is regarded as one of the polymer materials with potential for future AWH applications.

## Introduction

Although 70% of the earth's surface is covered by water, humans are currently facing an unprecedented water crisis since 21 century.<sup>[1-4]</sup> Only about 1.3% of the water covering the earth's surface is surface freshwater, of which 0.2% is stored in the air, about  $2 \times 10^{10}$  cubic meters.<sup>[5-6]</sup> This water in the air is ubiquitous in the form of saturated water (fog) and unsaturated water (water vapor), but is difficult to collect.<sup>[7]</sup> Capturing water from moist air is known as atmospheric water harvesting (AWH).<sup>[8-10]</sup> With the advantages of high ambient humidity and no need for liquefaction, fresh water can be obtained from metal spike arrays or large hydrophobic woven meshes during cold nights.<sup>[11-12]</sup> However, in most areas it is difficult to saturate the relative air humidity.<sup>[13]</sup> On the other hand, liquefaction and collection of unsaturated water vapor from air is even more difficult because liquefaction of water vapor and storage of fresh water are two independent processes that are difficult to reconcile when selecting and designing AWH materials.<sup>[14-16]</sup>

In recent years, crystalline porous materials such as metal-organic frameworks (MOFs)<sup>[17-20]</sup> and covalent organic frameworks (COFs)<sup>[21-24]</sup> have been widely reported for AWH applica-

tions. These materials have well-defined chemical and crystalline structures, so it is easy to study their structure-property relationships. However, powdered MOFs and COFs material do not have macroscopically stabilized shapes and need to be 'flattened' on the substrate to increase the contact area with air. Compared to other AWH materials, polymer hydrogels and/or their composites are widely used for not only freshwater production, but also sensing and direct air electrolysis for hydrogen production, due to their ease of preparation, low cost, and excellent compatibility.<sup>[25-29]</sup> There is a wide variety of hydrophilic monomer and/or polymer raw materials that have been used to prepare AWH materials, including monomers such as isopropylacrylamide (NAPAM), acrylamide (AM), and 2-(acryloyloxyethyl) trimethylammonium chloride (AEMA), as well as polymer precursors such as poly(vinyl alcohol) (PVA), chitosan, and others.<sup>[30-34]</sup> In addition, hygroscopic salts (e.g. calcium chloride, lithium chloride) and photothermal materials (e.g. graphene oxide, carbon nanotubes) have been incorporated into polymer matrix to boost the water productivity.<sup>[35-36]</sup> However, the relationship between the chemical structure of the raw materials and the water sorption/desorption properties of the resulting hydrogels has been overlooked, resulting in a lack of fair comparisons between state-of-the-art AWH systems to guide researchers in rationally designing AWH hydrogel materials, which may reduce the efficiency of the research and increase the experimental cost.<sup>[37-40]</sup>

In this study, we prepared a series of hydrogel AWH materials using various monomer raw materials and investigated the relationship between chemical structure and physicochemical properties of the resulting hydrogels, such as hydrogel swelling ratio, hydrogel pore size, vapor adsorption kinetics and electrostatic potential etc. We found that the AWH hydrogel prepared by cross-linking ionic monomers (e.g. AEMA, APtMA, and AMPS) exhibited high swelling ratio, dense pore structure, fast vapor adsorption and hence better AWH

[a] A. Feng, Y. Shi, C. Onggowarsito, X. S. Zhang, S. Mao, M. A.H. Johir, Q. Fu, L. D. Nghiem  
 Centre of Technology in Water and Wastewater, School of Civil and Environmental Engineering, University of Technology Sydney, NSW 2007, Australia  
 E-mail: Qiang.Fu@uts.edu.au

Supporting information for this article is available on the WWW under <https://doi.org/10.1002/cssc.202301905>

© 2024 The Authors. ChemSusChem published by Wiley-VCH GmbH. This is an open access article under the terms of the Creative Commons Attribution Non-Commercial License, which permits use, distribution and reproduction in any medium, provided the original work is properly cited and is not used for commercial purposes.

performance. Furthermore, we incorporated three photothermal materials (PTMs) into the PAMPS hydrogel, evaluated their water adsorption capacity and desorption efficiency and revealed the importance of the photothermal conversion performance of PTMs in AWH hydrogels. We thus expect that this study will provide guidance for the design and fabrication of high-performance AWH hydrogels in the future.

## Results and Discussion

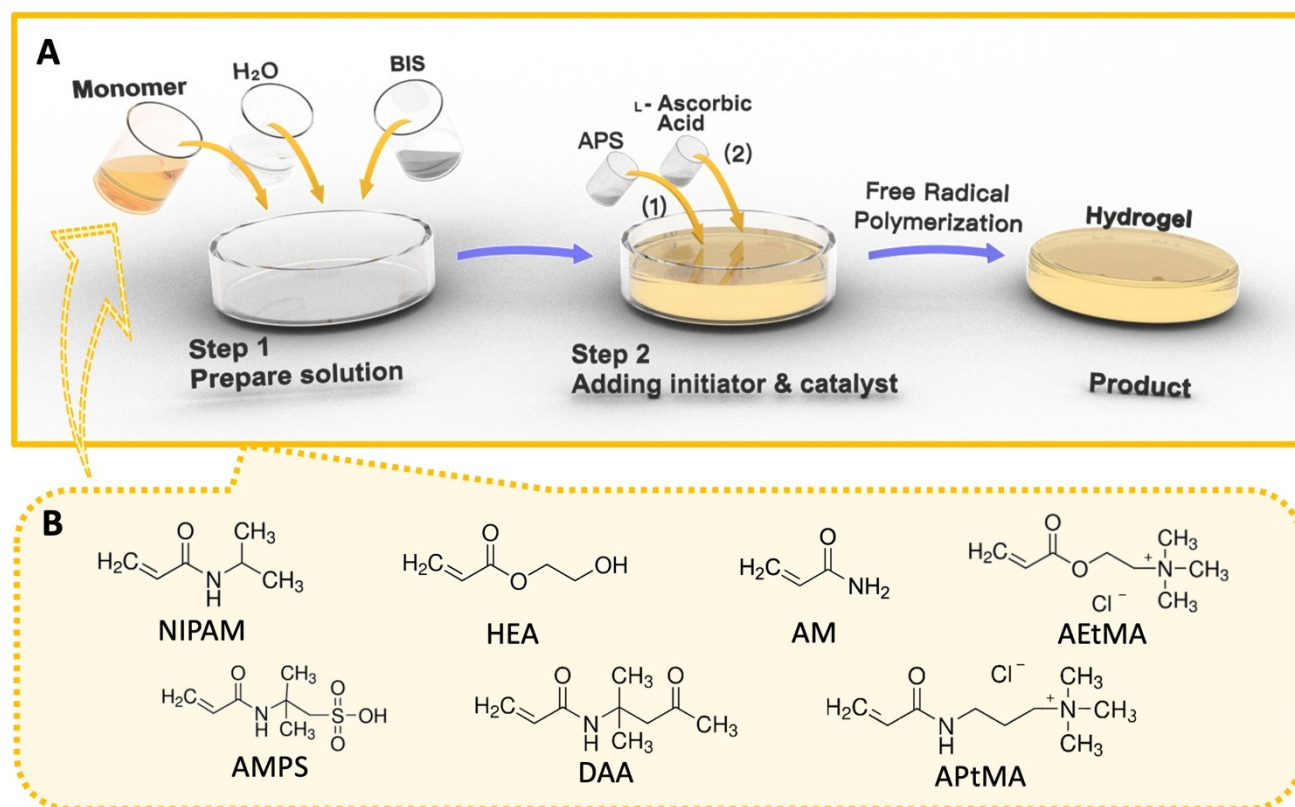
Current reports on AWH hydrogels usually overlook the effect of the structure-property-application relationships. Moreover, it is difficult to make an objective and fair comparison of the reported AWH performance since different test devices and/or methods are used in different laboratories. This thus leaves a knowledge gap in the field, hindering the development of high-performance AWH materials for practical applications. In this study, we prepared a series of AWH hydrogels by cross-linking different hydrophilic monomers, including NIPAM, AEtMA, APtMA, AM, AMPS, HEA and PDAA (Scheme 1). *N,N'*-methylene bis(acrylamide) (BIS) and ammonium persulfate (APS) were used as a crosslinker and radical initiator, respectively. We then synthesized the hydrogels via free radical polymerization of monomers and cross-linker. The hydrogel products were washed with DI water and freeze-dried for characterization as well as adsorption/desorption tests. This strategy ensures that the backbone structure of polymer chain is consistent/similar in

all hydrogels, with the pendant moieties differing, thus minimizing the effect of the backbone and allowing for a more targeted study of the influence of different hydrophilic groups on the hydrogel AWH properties.

After freeze-drying, we characterized the resulting AWH hydrogels by FTIR spectrometer to confirm their characteristic chemical structures. As shown in Figure 1A, the amide groups (C(=O)–NH) of PNIPAM, PDAA, PAPtMA, and PAMPS chains were confirmed at  $3,270\text{ cm}^{-1}$  (N–H stretch) and  $1,650\text{ cm}^{-1}$  (C=O stretch), respectively. We also observed the characteristic peaks at  $930\text{ cm}^{-1}$ ,  $1,490\text{ cm}^{-1}$ , and  $2,930\text{ cm}^{-1}$ , which can be attributed to the  $\text{N}^+\text{–C}$  and C–H stretching vibrations of the quaternary ammonium groups of PAEtMA, respectively. The strong peaks at  $1,250\text{ cm}^{-1}$  and  $1,725\text{ cm}^{-1}$  can be assigned to the ester groups (C(=O)–O) of PAEtMA and PHEA. The dried hydrogels have a diameter of 30 mm and a thickness of 3.5 mm, with an aspect ratio of 8.6 (Figure 1B).

A high porosity surface increases the air-solid contact area and facilitates the water adsorption at the interior interface of the hydrogel. We characterized the microporous structure of the hydrogels by scanning electron microscopy (SEM). We found that PAPtMA-, PAMPS-, PAEtMA-, PNIPAM-, PAM-, and PDAA-based hydrogels have porous structure with uniform pore size under the same preparation conditions (Figure 1C i–v&vii). While, small open pores were observed on the surface of PHEA hydrogels (Figure 1C vi).

In this study, Avogadro software was used to build molecular electrostatic potential maps of the repeating units of



**Scheme 1.** Illustration of the synthesis of AWH hydrogels. (A) Step-by-step procedure for hydrogel synthesis. (B) Chemical structures of different monomers.

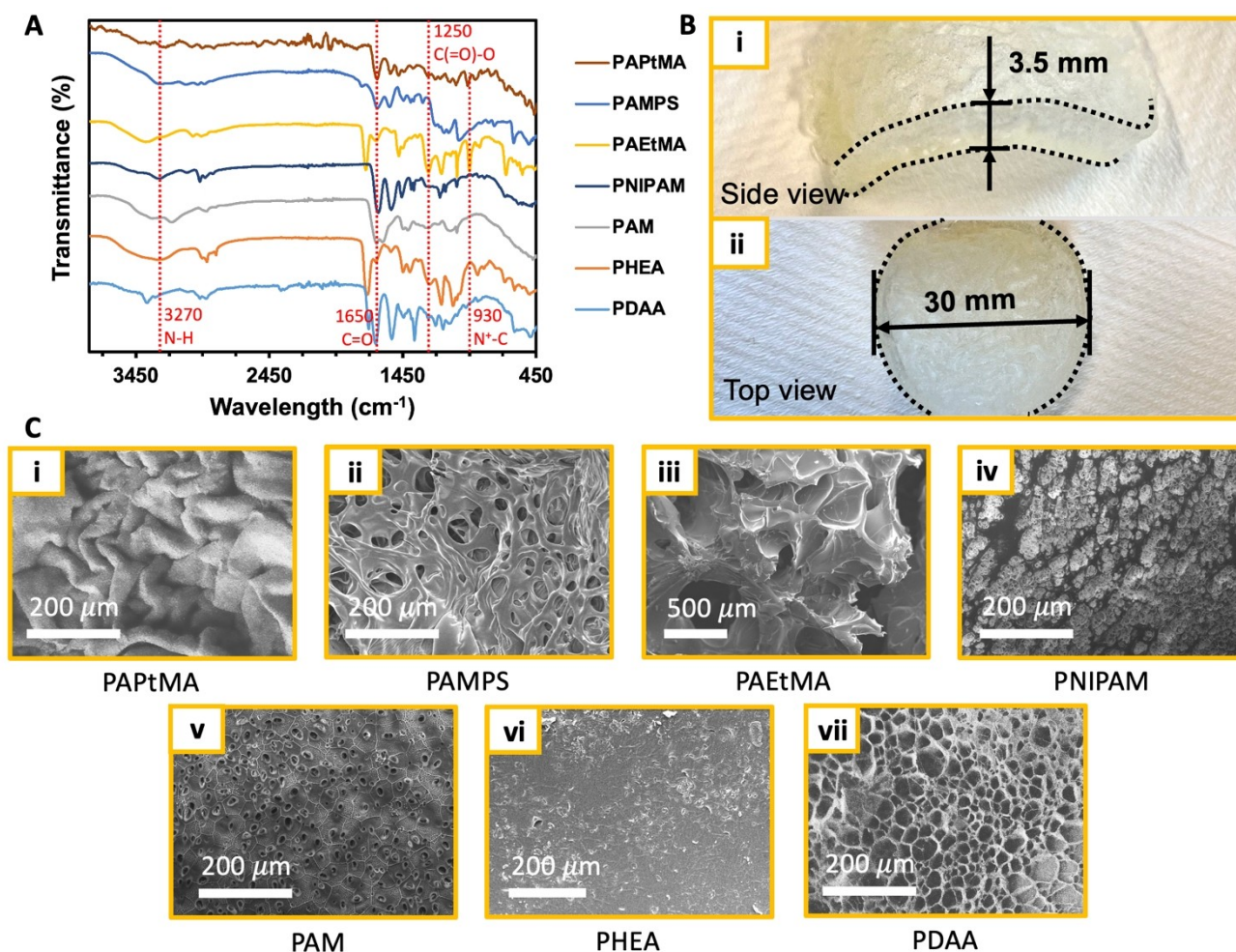


**Figure 1.** (A) FT-IR spectra of PAMPS, PHEA, PAM, PAEtMA, PNIPAM, PDAA, PDMA, and PAPTMA hydrogels. (B) Optic image of PAMPS hydrogel for size and aspect ratio illustration. (C) SEM images of (i) PAPTMA, (ii) PAMPS, (iii) PAEtMA, (iv) PNIPAM, (v) PAM, (vi) PHEA, and (vii) PDAA hydrogel surface.

hydrogels. The Merck Molecular Force Field (MMFF94) was used to simply simulate the electrostatic potentials using the steepest descent method. Water molecules are then introduced to random locations in the molecular model, and the total energy differences ( $\Delta E$ ) before and after the addition of water molecules were calculated (Figure S1). The energy difference is negative, which means that energy is released during the formation of hydrogen bonds between the polymer chains and the water molecules, and the enthalpy of the system decreases. That is, under conditions of random distribution of water molecules, the difference in the total energy of the system can be correlated with the driving force of water molecules on the polymer chains. As shown in Table 1, the PAPTMA hydrogel has the highest absolute value  $|\Delta E|$ , while PHEA and PDAA hydrogels have lower absolute values, which suggests that these two hydrogels have relatively low driven force when adsorbing water molecules.

In this study, we defined the hydrogel swelling ratio (SR) as the mass ratio of saturated hydrogel to the dry gel. Due to their stronger water affinity, the anionic PAMPS and cationic PAEtMA and PAPTMA hydrogels exhibited a higher SR of  $> 25$

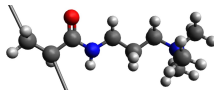
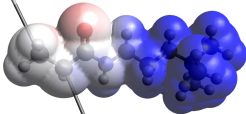
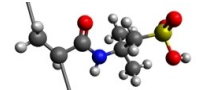
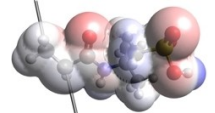
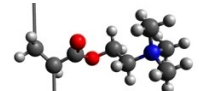
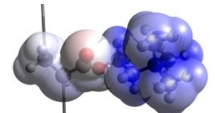
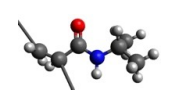
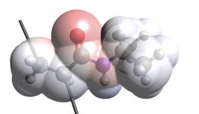
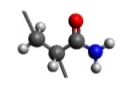
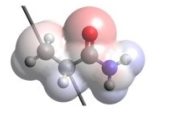
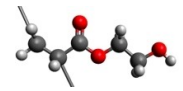
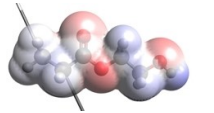
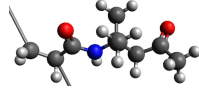
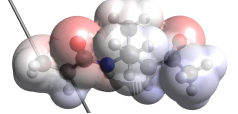
compared to other AWH hydrogels (Table 1). This result is attributed to their high polarity of pendant groups and their strong interaction with water molecules. For the neutral hydrogels, the PNIPAM has a relatively higher SR of 9.9 and the PDAA shows the lowest SR of 4.6. The SR values of the prepared AWH hydrogels are in the order of PAPTMA  $>$  PAMPS  $>$  PAEtMA  $>$  PNIPAM  $>$  PAM  $>$  PHEA  $>$  PDAA.

Finally, we plotted the SR versus  $|\Delta E|$  of AWH hydrogels. As seen in Figure S2, the  $|\Delta E|$  values of AWH hydrogels is nonlinearly related to their SR with a  $R^2$  of 0.9919. This result implies that the driving force for water absorption of hydrogels also correlates to the ultimate water storage capacity of the hydrogel to some extent.

The resulting dry hydrogels were then placed on a hydrophobic foam in a beaker containing DI water, and the static water adsorption test was carried out for 12 hours. The beaker is sealed with parafilm to isolate the outside air, and the humidity inside the beaker can be tuned by adjusting the temperature (see Figure S3A in Supporting Information). The weight of the hydrogel was recorded at different time intervals. The sorped water was then desorbed under solar irradiation



**Table 1.** Summary of AWH hydrogels with their chemical structure, electrostatic potential mapping, absolute value of electrostatic potential difference, and swelling ratio.

Monomer	Structure <sup>a</sup>	Electrostatic Potential Map <sup>b</sup>	EPD  <sup>c</sup> (kJ/mol)	Swelling Ratio (100%)
APtMA			3835	27.1
AMPS			3702	26.1
AEtMA			3420	24.6
NIPAM			1379	9.9
AM			848	6.9
HEA			732	5.2
DAA			550	4.6

<sup>a</sup> Grey: C; White: H; Red: O Blue: N and Yellow: S. <sup>b</sup> Electrostatic potential mapping: Blue: positive, Red: negative. <sup>c</sup> Absolute value of electro-potential difference.

(see Figure S3B in Supporting Information). Water evaporation rates and desorption efficiencies of all the AWH hydrogels were derived by measuring the mass change of the hydrogels every 30 minutes using a precision balance. Of particular note, the water adsorption performance of the AWH hydrogels are obtained by calculating the average of three cycles.

To quantify the water sorption performance of these AWH hydrogels, a 12-hour continuous water sorption test under 60% humidity was performed. Each sample was conducted three individual water adsorption/desorption experiment under the same conditions for greater accuracy. More detail on calculation and experimental methods are shown in Supporting Information S2.4. At the molecular level, charged hydrogels (i.e. PAEtMA, PAPtMA, and PAMPS) have a greater affinity for water molecules than uncharged ones, which explains why they have greater water sorption capacities than neutral hydrogels. The water sorption of hydrogels is, however, influenced by the type of ionic functional groups present in the “stationary” phase (polymer chains with fixed position). PAPtMA had the highest

water sorption capacity of  $0.634 \text{ g g}^{-1}$ , followed by PAMPS ( $0.621 \text{ g g}^{-1}$ ) and PAEtMA ( $0.482 \text{ g g}^{-1}$ ) (Figure 2A–C). The neutral hydrogels (i.e. PNIPAM, PAM, PHEA and PDAA) have low water uptake capacity of  $0.317 \text{ g g}^{-1}$ ,  $0.303 \text{ g g}^{-1}$ ,  $0.239 \text{ g g}^{-1}$  and  $0.237 \text{ g g}^{-1}$ , respectively. We also prepared a controlled hybrid hydrogel poly(AMPS-co-AEtMA) by copolymerizing AMPS and AEtMA monomers. Interestingly, the water adsorption capacity of poly(AMPS-co-AEtMA) hydrogel is  $0.5063 \text{ g g}^{-1}$ , which is between PAEtMA and PAMPS (Figure S4 in S2.5 Supporting Information). At molecular level we also found a relationship between the side-chain length and the water adsorption capacity. In Avogadro’s molecular simulations, the flexibility of the polymer backbone decreases with the increase of side chain length, which makes the hydrophilic functional groups on the side chains are completely exposed to the activity space of water molecules. On the other hand, the relative angles between the polymer side chains are not completely fixed. The side chain can point in any direction normal to the plane of the backbone direction (this is especially apparent when the ends

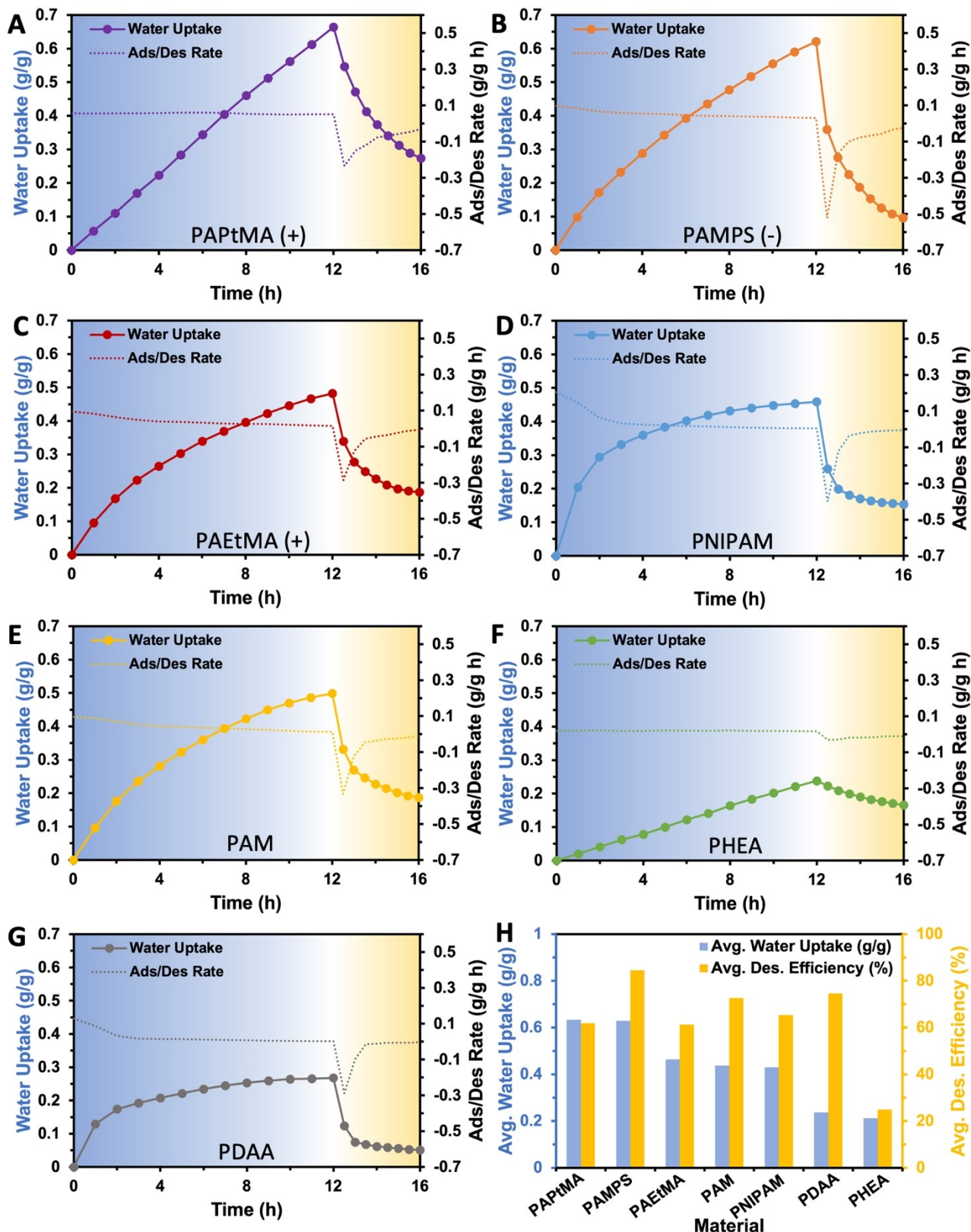


**Figure 2.** (A–G) 12 h water adsorption and 4 h water desorption curves and their adsorption/desorption rates of the AWH hydrogels, each sample were conducted three times for higher accuracy. Water desorption is conducted under  $1 \text{ kW m}^{-2}$  (1.0 sun equivalent). (H) Comparison of average water adsorption capacity and water desorption efficiency for AWH hydrogels.

of the side chains contain large hydrophilic functional groups, such as PAEtMA), which means that the spatial hinderance of water molecules to enter the space near the main chain is weakened, resulting in an increase in the water-absorbent properties of the polymer.

Under sunlight irradiation, all the AWH hydrogels showed a relatively high desorption efficiency of more than 60%, except for PHEA hydrogel. This result may be due to the near closure of the pores on its surface. Notably, during the desorption process the initial water desorption rates are in the order: PAMPS ( $0.43 \text{ g g}^{-1} \text{ h}^{-1}$ ) > PNIPAM ( $0.39 \text{ g g}^{-1} \text{ h}^{-1}$ ) > PAM ( $0.34 \text{ g g}^{-1} \text{ h}^{-1}$ ) > PAEtMA ( $0.28 \text{ g g}^{-1} \text{ h}^{-1}$ ) > PDAA ( $0.24 \text{ g g}^{-1} \text{ h}^{-1}$ ) > PAPtMA ( $0.23 \text{ g g}^{-1} \text{ h}^{-1}$ ) > PHEA ( $0.02 \text{ g g}^{-1} \text{ h}^{-1}$ ) (see Figure 2). Although PAPtMA has the best water adsorption performance, it showed a compromised desorption efficiency of 62%. The

desorption efficiency of PAMPS was much higher at 83% while still having good adsorption capacity, which means that PAMPS hydrogel are more advantageous in fast adsorption/desorption cycles compared to PAPtMA.

We then illustrate the structure-property-application relationships of the AWH hydrogels. We directly compared the water sorption driving forces determined by molecular simulations, experimentally obtained SRs and the water sorption capacities of the hydrogels. As seen from Figure 3, the PAPtMA hydrogel exhibited the highest SR value and the largest  $|\Delta E|$ , and therefore the highest water adsorption capacity, similar as PAMPS and PAEtMA. As expected, the SR and  $|\Delta E|$  of the neutral hydrogels PNIPAM, PAM, PHEA and PDAA gradually decreased, as did their water adsorption capacity. In Figure S2, the monochromatic region visually represents the product of SR

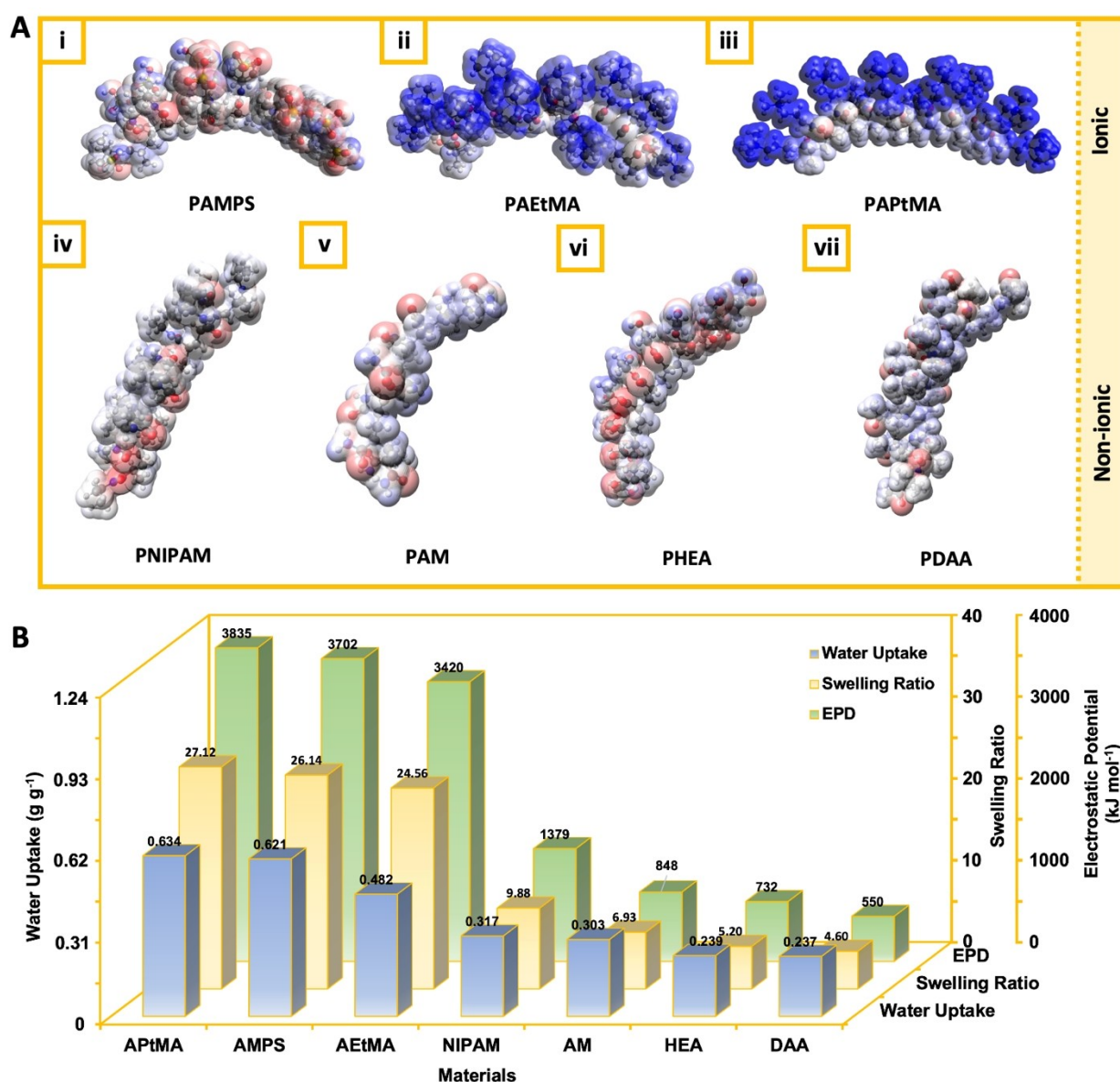


**Figure 3.** (A) Electrostatic potential difference of PAPtMA, PAMPS, PAEtMA, PNIPAM, PAM, PHEA and PDAA polymer chains (each polymer chain is presented with ten monomers for better trend illustration). Dark gray dots: carbon, light gray dots: hydrogen, blue dots: nitrogen, red dots: oxygen, yellow dots: sulfur. (B) Positive correlation of water adsorption capacity with the absolute value of electro-potential difference and swelling ratio of the hydrogels.



and  $|\Delta E|$  for AWH hydrogels. The area of this region is ranked in the following order of size: PAPTMA > PAMPS > PAEMA > PDMA > PNIPAM > PAM > PHEA > PDAA. Interestingly, this order is consistent with the trend of high to low AWH performance of the AWH materials. In all, this result indicates that the water sorption capacity of hydrogel is affected by both volumetric water swelling capacity and chemical structure.

It is particularly noteworthy that to develop high-performance AWH materials for practical applications, we need them to have balanced water adsorption capacity and desorption efficiency. After comprehensive consideration, PAMPS in this study is considered as the most promising AWH material. We next tested the water adsorption-desorption performance of

the PAMPS hydrogels under different relative humidity conditions, and demonstrated the excellent all-weather water adsorption capacity of PAMPS hydrogels under 30–90% R.H. conditions (Figure S5, S2.6 in Supporting Information). To further improve the desorption efficiency, we incorporated three PTMs into PAMPS hydrogel, including manganese-polydopamine nanoparticles (PDA(Mn)NPs) and carbon-based PTMs such as carbon nanotubes (CNTs) and graphene oxides (GOs). We found that the PAMPS+PTM composite hydrogels displayed a reduced water adsorption capacity. Among them, the water sorption capacity of PAMPS+GO hydrogel was reduced by 7% compared to the pristine PAMPS, followed by PAMPS+CNT (−9.5%) and PAMPS+PDA(Mn)NPs (−15%) (Figure 4A),

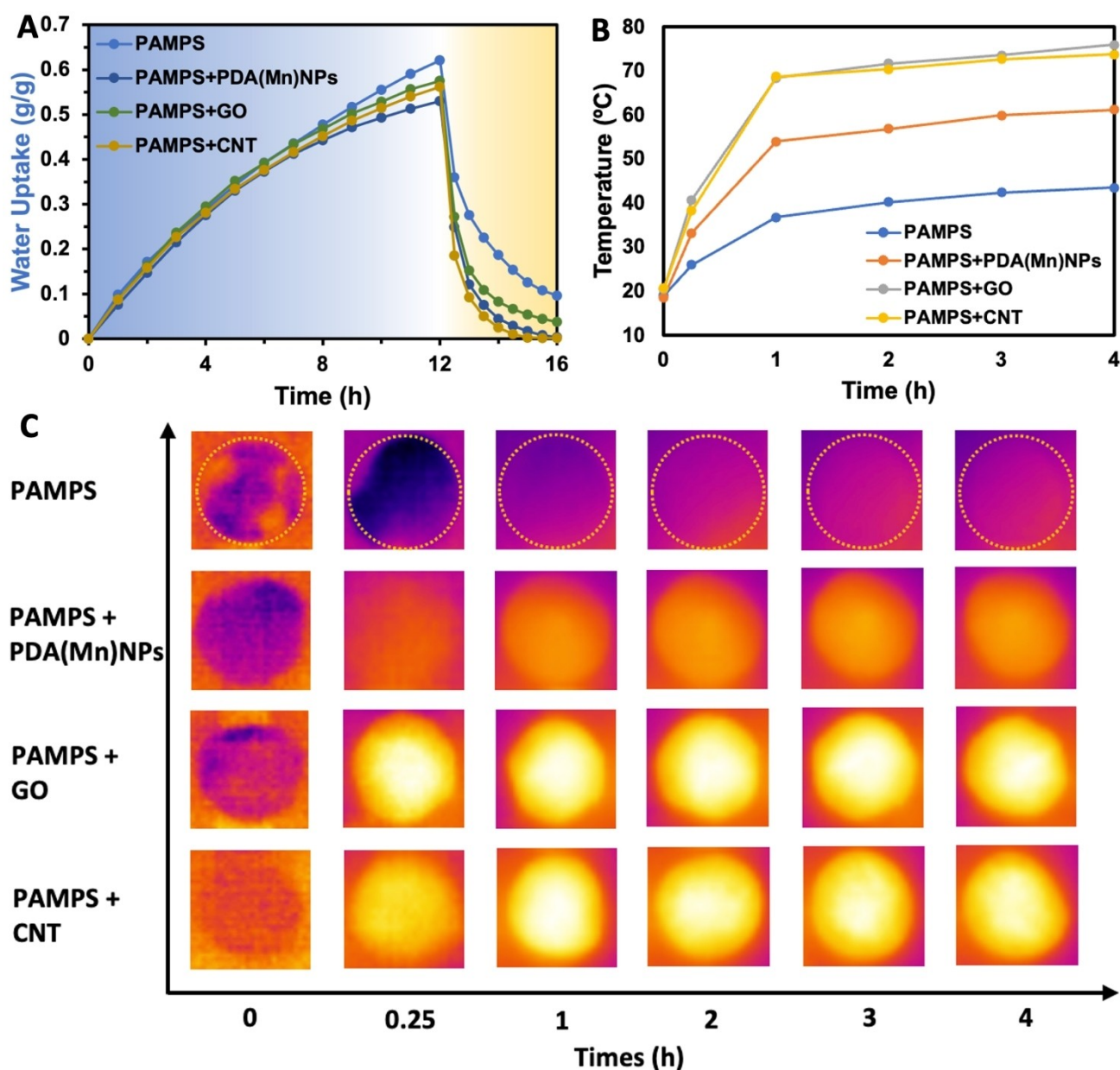


**Figure 4.** (A) Water adsorption and desorption process of PAMPS hydrogel with PDA(Mn)NPs, GO, and CNT as photothermal converter. (B) Temperature changing with sunlight irradiation time of PAMPS hydrogel with PDA(Mn)NPs, GO, and CNT as photothermal converter. (C) Infrared images of PAMPS hydrogel with PDA(Mn)NPs, GO, and CNT as photothermal converter at 0 h, 0.25 h, 1 h, 2 h, 3 h, and 4 h of sunlight irradiation.

since the PTMs display a lower adsorption capacity ( $<0.1 \text{ g g}^{-1}$ ) compared to PAMPS hydrogel, the resulting composite gels had a reduced water absorption capacity. The water adsorption rate of these composite hydrogels are also provided in Figure S6 (S2.7 in Supporting Information). All composite hydrogels exhibited excellent solar-to-heat conversion. Specifically, after 4 hours of continuous light exposure, the temperature of PAMPS+GO hydrogel reached an astonishing  $75.9^\circ\text{C}$ , followed by PAMPS+CNT hydrogel ( $73.7^\circ\text{C}$ ), PAMPS+PDA(Mn)NPs hydrogel ( $61.2^\circ\text{C}$ ) and pristine PAMPS hydrogel ( $40.3^\circ\text{C}$ ) (Figure 4B). The infrared images also recorded the temperature changes of the composite hydrogels (Figure 4C). The UV-Vis-NIR spectrum are also provided in Figure S7 (S2.8 in Supporting Information). In the wavelength range of 300–1900 nm, the light absorption of GO is significantly stronger than that of CNT. However, in the 1900–2400 nm range CNT can absorb more electromagnetic wave energy. As a result, the photothermal conversion performance of CNTs was the most pronounced during the desorption of water, and the water desorption rate of the PAMPS+CNT is  $0.75 \text{ g g}^{-1} \text{ h}^{-1}$ . Although the incorporation of GOs also increased the temperature of the hydrogel to  $75.9^\circ\text{C}$ , the desorption rate of PAMPS+GO was  $0.61 \text{ g g}^{-1} \text{ h}^{-1}$ . We hypothesized that the large number of oxygen-containing

functional groups in GO (e.g. epoxy, hydroxyl and carbonyl groups) formed additional H-bonding with water molecules, leading to reduced evaporation rate. In addition, the thermal stability of the two composite hydrogels (PAMPS+GO and PAMPS+CNT) was tested by three 24-hour sun exposure tests (1.0 solar equivalent). As shown in Figure S8, the surface temperatures of both samples reached above  $70^\circ\text{C}$  after 24 hours irradiation (1.0 sun equivalent). Moreover, both composite hydrogels retained their structural integrity after three cycles of irradiation, which indicates their extremely high thermal stability.

Finally, the outdoor water production test of PAMPS hydrogel was conducted in June 28–29, 2023, Ultimo, NSW, Australia, from 16:00 on June 28, 2023 to 6:00 on June 29, 2023. During the practical test, the temperature was basically maintained at about  $11^\circ\text{C}$ , the wind speed gradually increased from  $3.6 \text{ m s}^{-1}$  to about  $7.7 \text{ m s}^{-1}$ , the R.H. gradually decreased to 67%, and the dew point changed with the change of relative humidity (Figure 5A). The water production device used in pretrial experiment is shown in Figure 5B, with actual digital image showed in Figure S9. A PAMPS hydrogel achieved a water sorption capacity of  $0.42 \text{ g g}^{-1}$  in 8 hours and then released 85% of captured water under sunlight irradiation. We then

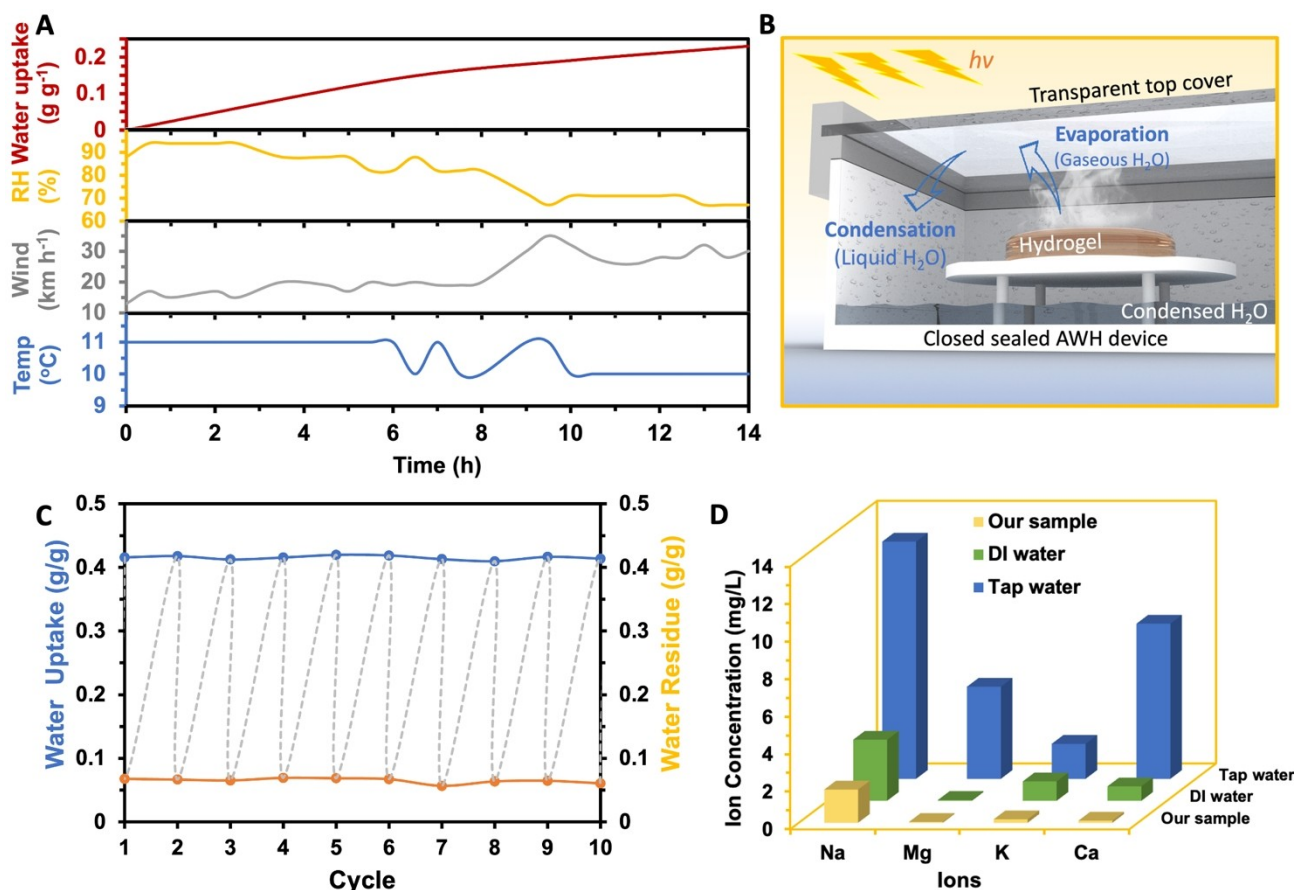


**Figure 5.** (A) Actual change of temperature, wind speed, relative humidity, and water adsorption data of PAMPS hydrogel at 28th June 2023, location at Ultimo of New South Wales, Australia. Original weather data is obtained from The Bureau of Meteorology of Australian Government, presented by Apple Weather application (iOS version: 16.6). (B) Water desorption device used in pretrial experiment. (C) AWH performance of PAMPS hydrogel in 10-times cycling tests. (D) ICP-MS ions concentration analysis graph for commonly water-soluble ions.



tested the performance stability of PAMPS hydrogel in cycling tests and found that the PAMPS hydrogel is mechanically robust enough to support long-term (i.e. over 120 hours) continuous water sorption/desorption cycles without performance degradation. Its water adsorption capacity maintained at 0.42 g g<sup>-1</sup> after 10 water adsorption/desorption cycles (Figure 5C). Moreover, we analyzed the ions concentrations of the collected water. The concentrations of sodium, magnesium, potassium, and calcium ions in the collected water are significantly lower than DI water and Sydney Tap water (Figure 5D), and fully met the drinking water standards stipulated by the World Health Organization (WHO). This result demonstrates that PAMPS hydrogels have great potential in the field of AWH application.

## Conclusions

In conclusion, we evaluated a series of hydrogels for atmospheric water harvesting and systematically investigated their water sorption mechanisms and desorption kinetics. Based on scanning electron microscopy analysis, electrostatic potential mapping, and water sorption/desorption curves, we determined the impact of the chemical structure on AWH performance of hydrogels. The electrostatic potential difference provides the driving force for water sorption in hydrogels, and the swelling ratio also has a significant impact on the water sorption capacity of AWH hydrogels. We also studied the effect of the PTMs on the desorption efficiency of hydrogels. This study thus provide new insights to elucidate the current research gap in structure-property-application relationships and provide research directions for the design and synthesis of hydrogel-based AWH materials.

## Supplementary data

Information associated with this article can be found in the Supplementary material.

## Acknowledgements

Q. F. acknowledges the Australian Research Council under the Future Fellowship (FT180100312). A. F. acknowledges support of the International Research Scholarship from the University of Technology Sydney. Open Access publishing facilitated by University of Technology Sydney, as part of the Wiley - University of Technology Sydney agreement via the Council of Australian University Librarians.

## Conflict of Interests

The authors declare no conflicts of interest.

## Data Availability Statement

The data that support the findings of this study are available from the corresponding author upon reasonable request.

**Keywords:** Material selection · Swelling ratio · Water uptake · Free radical polymerization · Sunlight irradiation

- [1] M. N. Sharif, H. Haider, A. Farahat, K. Hewage, R. Sadiq, *Environ. Rev.* **2019**, *27*, 519–544.
- [2] J. Nycander, M. Hieronymus, F. Roquet, *Geophys. Res. Lett.* **2015**, *42*, 7714–7721.
- [3] D. Vollmer, I. J. Harrison, *Environ. Res. Lett.* **2021**, *16*, 011005.
- [4] V. Srinivasan, E. F. Lambin, S. M. Gorelick, B. H. Thompson, S. Rozelle, *Water Resour. Res.* **2012**, *48*, W10516.
- [5] J. Y. Suen, M. T. Fang, P. M. Lubin, *IEEE Trans. Terahertz Sci. Technol.* **2014**, *4*, 86–100.
- [6] C. Prigent, C. Jimenez, P. Bousquet, *J. Geophys. Res. Atmos.* **2020**, *125*, e2019JD030711-n/a.
- [7] V. G. Gude, *Rev. Environ. Sci. Bio/Technol.* **2017**, *16*, 591–609.
- [8] D. T. Degefie, T. S. El-Madany, M. Held, J. Hejkal, E. Hammer, J. C. Dupont, M. Haefefflin, E. Fleischer, O. Klemm, *Atmos. Res.* **2015**, *164–165*, 328–338.
- [9] N. Hanikel, M. S. Prévot, O. M. Yaghi, *Nat. Nanotechnol.* **2020**, *15*, 348–355.
- [10] A. Entezari, O. C. Esan, X. Yan, R. Wang, L. An, *Adv. Mater.* **2023**, *35*, e2210957-n/a.
- [11] F. Deng, Z. Chen, C. Wang, C. Xiang, P. Poredoš, R. Wang, *Adv. Sci.* **2022**, *9*, 2204724-n/a.
- [12] Z. Chen, S. Song, B. Ma, Y. Li, Y. Shao, J. Shi, M. Liu, H. Jin, D. Jing, *Sol. Energy Mater. Sol. Cells* **2021**, *230*, 111233.
- [13] M. G. Gado, M. Nasser, A. A. Hassan, H. Hassan, *Process Saf. Environ. Prot.* **2022**, *160*, 166–183.
- [14] X. Zhou, H. Lu, F. Zhao, G. Yu, *ACS Materials Lett.* **2020**, *2*, 671–684.
- [15] H. Lu, W. Shi, Y. Guo, W. Guan, C. Lei, G. Yu, *Adv. Mater.* **2022**, *34*, e2110079-n/a.
- [16] W. Shi, W. Guan, C. Lei, G. Yu, *Angew. Chem. Int. Ed.* **2022**, *61*, e202211267-n/a.
- [17] F. Fathieh, M. J. Kalmutzki, E. A. Kapustin, P. J. Waller, J. Yang, O. M. Yaghi, *Sci. Adv.* **2018**, *4*, eaat3198-n/a.
- [18] Y. Hu, Z. Fang, X. Ma, X. Wan, S. Wang, S. Fan, Z. Ye, X. Peng, *Appl. Mater. Today* **2021**, *23*, 101076.
- [19] H. Furukawa, F. Gándara, Y.-B. Zhang, J. Jiang, W. L. Queen, M. R. Hudson, O. M. Yaghi, *J. Am. Chem. Soc.* **2014**, *136*, 4369–4381.
- [20] H. Kim, S. Yang, S. R. Rao, S. Narayanan, E. A. Kapustin, H. Furukawa, A. S. Umans, O. M. Yaghi, E. N. Wang, *Science* **2017**, *356*, 430–434.
- [21] L. H. Chen, W. K. Han, X. Yan, J. Zhang, Y. Jiang, Z. G. Gu, *ChemSusChem* **2022**, *15*, e202201824-n/a.
- [22] H. L. Nguyen, *Adv. Mater.* **2023**, *35*, e2300018-n/a.
- [23] Y. Liu, W.-K. Han, W. Chi, J.-X. Fu, Y. Mao, X. Yan, J.-X. Shao, Y. Jiang, Z.-G. Gu, *Appl. Catal. B* **2023**, *338*, 123074.
- [24] S. Jiang, L. Meng, W. Ma, G. Pan, W. Zhang, Y. Zou, L. Liu, B. Xu, W. Tian, *Mater. Chem. Front.* **2021**, *5*, 4193–4421.
- [25] N. Li, L. Luo, C. Guo, J. He, S. Wang, L. Yu, M. Wang, P. Murto, X. Xu, *Chem. Eng. J.* **2022**, *431*, 134144.
- [26] X. Sun, S. Agate, K. S. Salem, L. Lucia, L. Pal, *ACS Appl. Bio Mater.* **2021**, *4*, 140–162.
- [27] X. Qu, J. Liu, S. Wang, J. Shao, Q. Wang, W. Wang, L. Gan, L. Zhong, X. Dong, Y. Zhao, *Chem. Eng. J.* **2023**, *453*, 139785.
- [28] H. Sai, A. Erbas, A. Dannenhoffer, D. Huang, A. Weingarten, E. Siismets, K. Jang, K. Qu, L. C. Palmer, M. Olvera de la Cruz, S. I. Stupp, *J. Mater. Chem. A* **2020**, *8*, 158–168.
- [29] P. Verma, A. Singh, F. A. Rahimi, T. K. Maji, *J. Mater. Chem. A* **2021**, *9*, 1368–13614.
- [30] F. Zhao, X. Zhou, Y. Liu, Y. Shi, Y. Dai, G. Yu, *Adv. Mater.* **2019**, *31*, e1806446-n/a.
- [31] G. Yilmaz, F. L. Meng, W. Lu, J. Abed, C. K. N. Peh, M. Gao, E. H. Sargent, G. W. Ho, *Sci. Adv.* **2020**, *6*, eabc8605-n/a.
- [32] R. Li, Y. Shi, M. Alsaedi, M. Wu, L. Shi, P. Wang, *Environ. Sci. Technol.* **2018**, *52*, 11367–11377.
- [33] M. Wu, R. Li, Y. Shi, M. Altunkaya, S. Aleid, C. Zhang, W. Wang, P. Wang, *Mater. Horiz.* **2021**, *8*, 1518–1527.

- [34] A. Entezari, M. Ejeian, R. Wang, *ACS Mater. Lett.* **2020**, *2*, 471–477.
- [35] P. A. Kallenberger, M. Fröba, *Commun. Chem.* **2018**, *1*, 28-n/a.
- [36] A. Feng, S. Mao, C. Onggowarsito, G. Naidu, W. Li, Q. Fu, *ACS Sustainable Chem. Eng.* **2023**, *11*, 5819–5825.
- [37] T. Li, T. Yan, P. Wang, J. Xu, X. Huo, Z. Bai, W. Shi, G. Yu, R. Wang, *Nat. Water* **2023**, *1*, 971–981.
- [38] T. Li, M. Wu, J. Xu, R. Du, T. Yan, P. Wang, Z. Bai, R. Wang, S. Wang, *Nat. Commun.* **2022**, *13*, 6771–6771.
- [39] J. Xu, T. Li, T. Yan, S. Wu, M. Wu, J. Chao, X. Huo, P. Wang, R. Wang, *Energy Environ. Sci.* **2021**, *14*, 5979–5994.
- [40] J. Xu, T. Li, J. Chao, S. Wu, T. Yan, W. Li, B. Cao, R. Wang, *Angew. Chem.* **2020**, *132*, 5240–5248.

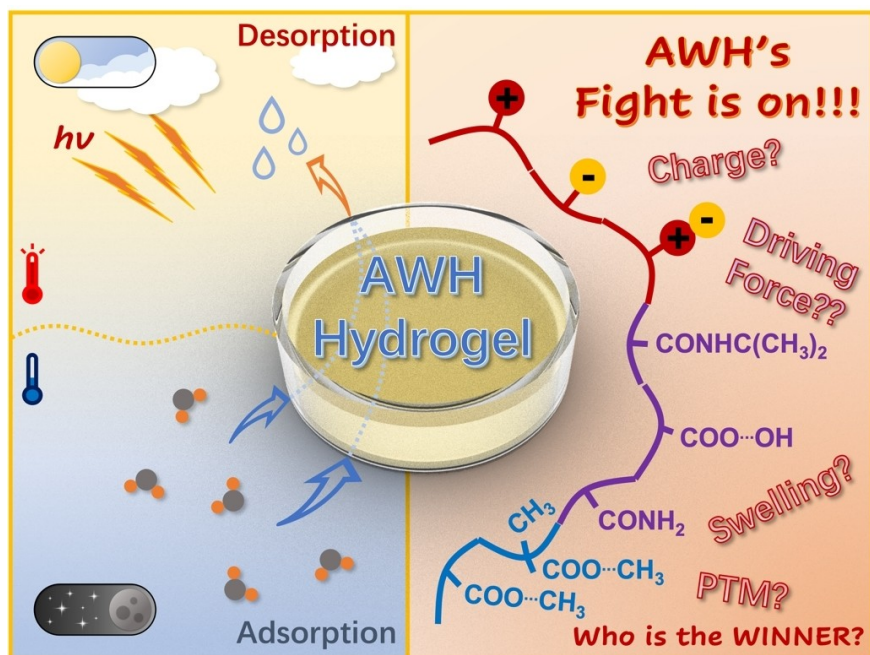
---

Manuscript received: December 19, 2023

Revised manuscript received: January 16, 2024

Accepted manuscript online: January 24, 2024

Version of record online: ■■, ■■



A. Feng, Y. Shi, C. Onggowarsito, X. S. Zhang, S. Mao, M. A.H. Johir, Q. Fu\*, L. D. Nghiem

1 – 11

Structure-Property Relationships of Hydrogel-based Atmospheric Water Harvesting Systems

Through comparing the relationship among water adsorption capacity, swelling ratio, and absolute value of the electrostatic potential difference, the physical and chemical properties of AWH hydrogel were well-investi-

gated. The selected PAMPS hydrogel manages to have a  $0.62 \text{ g g}^{-1}$  of water uptake at 60%RH environment, as well as a 84.54% water desorption efficiency.